ACS APPLIED MATERIALS & INTERFACES

Research Article

www.acsami.org

Optoelectronic Properties of a Fullerene Derivative Containing Adamantane Group

Xia-Xia Liao,[†] Taishan Wang,*[,‡,§] Jizheng Wang,[§] Jin-Cheng Zheng,*[,†] Chunru Wang,[§] and Vivian Wing-Wah Yam*[,‡]

[†]Department of Physics, and Institute of Theoretical Physics and Astrophysics, Xiamen University, Xiamen, 361005, P. R. China

[‡]Department of Chemistry, The University of Hong Kong, Pokfulam Road, Hong Kong, P. R. China

[§]Beijing National Laboratory for Molecular Sciences, Institute of Chemistry, Chinese Academy of Sciences, Beijing, 100190, P. R. China

Supporting Information

ABSTRACT: A fullerene derivative linked with an adamantane cage, [6,6]-phenyl-C_{61}-butyric acid 1-adamantane methyl ester ($PC_{61}BAd$), has been designed and synthesized. Systematic investigations on its organic field effect performance, photovoltaic properties, and corresponding thermal stability have been made. In OFET device, the electron mobility (μ_e) of $PC_{61}BAd$ was found to reach a value as high as 0.01 $cm^2/V{\cdot}s$ with a high on-off (I_{on}/I_{off}) ratio of 4.9×10^6 that is useful for logic device applications. In the organic photovoltaic devices of P3HT:$PC_{61}BAd$, the power conversion efficiency (PCE) was found to reach 3.31 % in the optimized device. More importantly, the active layer of P3HT:$PC_{61}BAd$ was found to exhibit superior thermal stability over that of P3HT:$PC_{61}BM$. After heating at 150 °C for 20 h, the P3HT:$PC_{61}BAd$ device still showed a PCE of 2.44 %, demonstrating the applicability of $PC_{61}BAd$ as an acceptor material for the preparation of thermally stable organic solar cells. X-ray diffraction and atomic force microscopy were employed to probe the structure and morphology of $PC_{61}BAd$ and to rationalize its performance as an organic electronic material.

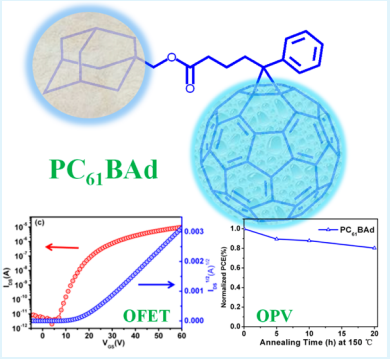

KEYWORDS: *fullerene derivative, field effect transistor, organic photovoltaics, adamantane, thermal stability*

INTRODUCTION

Organic electronics have attracted much attention due to their potential applications in the development of nanoelectronics and devices. They possess advantages such as low-cost fabrication, light weight, and high mechanical flexibility.[1−6] Fullerene derivatives represent an important family of n-type semiconductors for various electronic applications.[7−9] Because of the presence of π-conjugation, fullerene derivatives exhibit high electron affinity and strong carrier transport ability, thereby acting as excellent electronic materials and acceptors in organic photovoltaic (OPV) devices.[10−12] In the field of organic field effect transistors (OFETs) and organic solar cells (OSCs), [6,6]-phenyl-C_{61}-butyric acid methyl ester ($PC_{61}BM$) and its corresponding C_{70} derivative $PC_{71}BM$ are widely used and represent an important class of organic semiconductors. The electron mobility of $PC_{61}BM$-based OFETs reaches values as high as ~0.2 $cm^2/V{\cdot}s$ after device optimization and the PCE of P3HT:$PC_{61}BM$ OSCs approaches 5 %.[9,13−16] However, the high diffusion mobility and possible aggregation of $PC_{61}BM$ will normally lead to large clusters or micro-crystals in the films, which could cause poor phase separation in the donor/acceptor mixed films, influencing the performance of their corresponding OSCs.[12] Therefore, there is a strong need to find ways to improve the stability of these organic semiconductors.

Adamantane is a highly symmetrical molecule consisting of fused cyclohexanes in the chair conformation. Incorporation of the adamantane unit into polymers has been shown to significantly improve the stability of polymers, such as enhancing their heat-resistant property and glass transition temperature.[17−19] The enhanced stability of these polymers is mainly due to the symmetrical and inert cage structure of adamantane and its high hydrophobicity, which prevents degradation reactions, such as those involving oxidation or elimination. However, its effects on the properties of fullerene semiconductors and OPV devices have not yet been explored. Herein are described the design and synthesis of a new fullerene derivative ($PC_{61}BAd$) with an adamantane cage. $PC_{61}BAd$ has been demonstrated to display unique field effect performance and photovoltaic properties. The electron mobility of $PC_{61}BAd$ in OFET has been found to reach 0.01 $cm^2/V{\cdot}s$ with a high I_{on}/I_{off} ratio of 4.9×10^6. In OPV devices, the PCE was found to reach 3.31 % in an optimized device. More importantly, $PC_{61}BAd$-based OPV devices exhibit superior thermal stability over that of the $PC_{61}BM$-based devices. X-ray diffraction and atomic force microscopy were employed to

Received: June 28, 2013
Accepted: September 16, 2013
Published: September 27, 2013

probe the structure and morphology of $PC_{61}BAd$ and to rationalize its performance as an organic electronic material.

EXPERIMENTAL SECTION

Synthesis. $PC_{61}BAd$ was synthesized by the reaction of $PC_{61}BM$ (200 mg, 0.22 mmol) with 1-adamantane methanol (73 mg, 0.44 mmol) catalyzed by *p*-toluenesulfonic acid (38 mg, 0.22 mmol) in toluene solution (200 ml) at 120 °C for 24 h. $PC_{61}BAd$ was isolated by high-performance liquid chromatography (HPLC) using Buckyprep column. The identity of $PC_{61}BAd$ was confirmed by the matrix assisted laser desorption ionization-time of flight (MALDI-TOF) mass spectrometry and NMR spectroscopy (see Supporting Information for characterization data Figures S1−S8).

Device Fabrication and Characterization. N-Doped silicon with 300 nm silicon dioxide (n^{++}-Si/SiO_2) wafer was used as the bottom gate/insulator in the OFET. The Si/SiO_2 substrates were cleaned with deionized water, acetone and ethanol. The substrates were then treated with the silane-coupling reagent, hexamethyldisilazane (HMDS, purchased from Aldrich), in a vacuum oven for 3 h for comparison study with the bare Si/SiO_2. The prepared $PC_{61}BAd$ solution (10 mg/mL) in chloroform was spin-coated on the HMDS treated Si/SiO_2 and the bare Si/SiO_2 substrates in a N_2 glove box at a speed of 2000 rpm for 30 s. After being annealed at 150 °C for 10 min, a bilayer of Ca/Al (20 nm/40 nm) was vacuum-deposited through a shadow mask on the top of the semiconductor as the source and drain electrodes. The electrodes were designed as an interdigitated structure with a channel length (L) of 80 μm and width (W) of 8800 μm. The performances of the OFETs were characterized by the Keithley 4200 source meter in the N_2 glove box at room temperature.

The structure of the OSC was made up of indium tin oxide (ITO)/poly(3,4-ethylenedioxythiophene):poly(styrenesulfonate) (PEDOT:PSS) (Baytron P VPAI 4083)/P3HT:$PC_{61}BAd$/Ca/Al. The ITO glasses were pre-cleaned by sequential ultrasonic treatment in deionized water, acetone and isopropyl alcohol for 10 min each and then treated with oxygen plasma for 6 min. The PEDOT: PSS was filtered through a 0.45-μm filter and spin-coated at 3000 rpm for 30 s on the ITO layer. After baking at 140 °C for 10 min in air, the substrates were transferred into the N_2 glove box. The blend solutions of P3HT:$PC_{61}BAd$ with various ratios (1:0.4, 1:0.6, 1:0.8, 1:1, 15 mg/mL polymer) in dichlorobenzene (DCB) were spin-coated onto the PEDOT: PSS layer at a speed of 1200 rpm for 18 s. Then the active layers were baked at 110 °C for 10 min in N_2. The active layer thicknesses of the four devices in various ratios (1:0.4, 1:0.6, 1:0.8, 1:1) detected by an Ambios Technology XP-2 surface profilometer were approximately 95, 110, 130, and 170 nm. For the thermal stability characterization, the active layers were baked at 150 °C for 5, 10, and 20 h at a P3HT/$PC_{61}BAd$ ratio of 1:0.6. A cathode of 20 nm/60 nm Ca/Al was vacuum-evaporated. For comparison studies, the devices of P3HT:$PC_{61}BM$ (1:0.8, 15 mg/mL polymer) were fabricated at a speed of 500 rpm for 18 s with the same treatment. The active layer thickness of the P3HT:PCBM device was about 200 nm. The current density-voltage (J−V) characteristics were measured under simulated sunlight of a 450 W Newport 6279 NS solar simulator. The simulated solar light was calibrated to match 100 mW cm^{-2} level (AM 1.5G) by a standard mono-crystalline silicon solar cell. The external quantum efficiency (EQE) was measured using an Oriel IQE-200 instrument.

The optical microscopic images were obtained with an Olympus BX51 microscope. The X-ray diffraction (XRD) patterns of active layers were characterized by a Bruker D8 Advance Diffractometer with Cu K_α (λ = 1.5406 Å). The morphology of the active layers was measured by atomic force microscopy (AFM) in air using a Nanoscope III probe in tapping mode.

RESULTS AND DISCUSSION

The structures of $PC_{61}BAd$, $PC_{61}BM$, and P3HT are shown in Figure 1 along with the configurations of the OFET and solar cell devices.

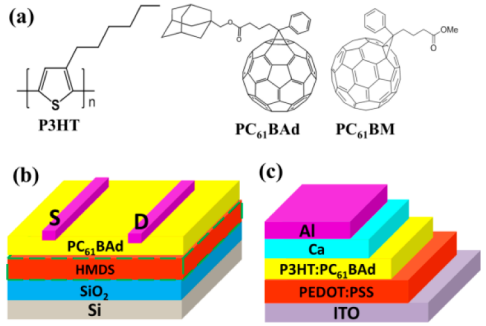

Figure 1. (a) Structures of P3HT, $PC_{61}BAd$, and $PC_{61}BM$; (b) structure of the OFET; (c) structure of the OSC.

Chemical Properties. $PC_{61}BAd$ consists of an adamantane group that takes up the position of the methyl group in $PC_{61}BM$. The highly hydrophobic nature of the adamantane group has rendered $PC_{61}BAd$ highly soluble in most common organic solvents. Electrochemical behaviours of $PC_{61}BAd$ and $PC_{61}BM$ were examined by cyclic voltammetry (CV) (Figure S2). $PC_{61}BAd$ displays a similar lowest unoccupied molecular orbtial (LUMO) level (−3.67 eV) as that of $PC_{61}BM$ (−3.66 eV).[6] This indicates that the adamantane cage has little influence on the LUMO level of the methanofullerene, in line with the lack of electron-donating groups or π-conjugation on the adamantane group, giving rise to the similar molecular orbital levels of $PC_{61}BAd$ as those of $PC_{61}BM$. The UV-vis absorption spectra were recorded in toluene (Figure S3), with $PC_{61}BAd$ exhibiting a slightly stronger absorption than that of $PC_{61}BM$ in the range between 300 and 400 nm. The rather similar electronic absorption patterns of $PC_{61}BAd$ and $PC_{61}BM$ are mainly originated from the domination of the π−π^* transitions of the fullerene moiety in both derivatives.

Field Effect Performance. The structure of OFET is shown in Figure 1b. Two kinds of OFETs are fabricated, one with and one without the HMDS modification layer. The performance of both devices is optimized by varying the annealing temperature for the $PC_{61}BAd$ films, and 150 °C is found to be optimal for both.

Figure 2 shows the transfer and output characteristics of the OFETs. It can be seen that for both devices without (Figure 2a,b) and the one with HMDS (Figure 2c,d), *n*-type characteristics with linear and saturation regimes are clearly displayed. According to the equation[20]

$$I_{DS} = \left(\frac{W}{2L}\right)\mu_e C_i (V_{GS} - V_T)^2$$

(where I_{DS} is the drain current, C_i is the capacitance per unit area of the gate dielectric, V_{GS} and V_T are the respective gate voltage and threshold voltage), the electron saturation mobility for the device without HMDS is calculated to be 8.85×10^{-4} $cm^2/V{\cdot}s$ (with I_{on}/I_{off} ratio of 6×10^5 and V_T of 3.6 V), and the electron saturation mobility for the device with HMDS is calculated to be 0.01 $cm^2/V{\cdot}s$ (with I_{on}/I_{off} ratio of 4.9×10^6 and V_T of 18.7 V), about 11 times higher than that of the device without HMDS (Table 1). In addition, the I_{on}/I_{off} ratio of 4.9×10^6 for $PC_{61}BAd$ with HMDS has also been increased by almost one order of magnitude compared to that of $PC_{61}BM$ (6×10^5). The enhanced performance of the devices in the presence of HMDS may arise from the hydrophobic nature of HMDS which would lead to the formation of a hydrophobic surface, which is beneficial for film crystallization.[21−23]

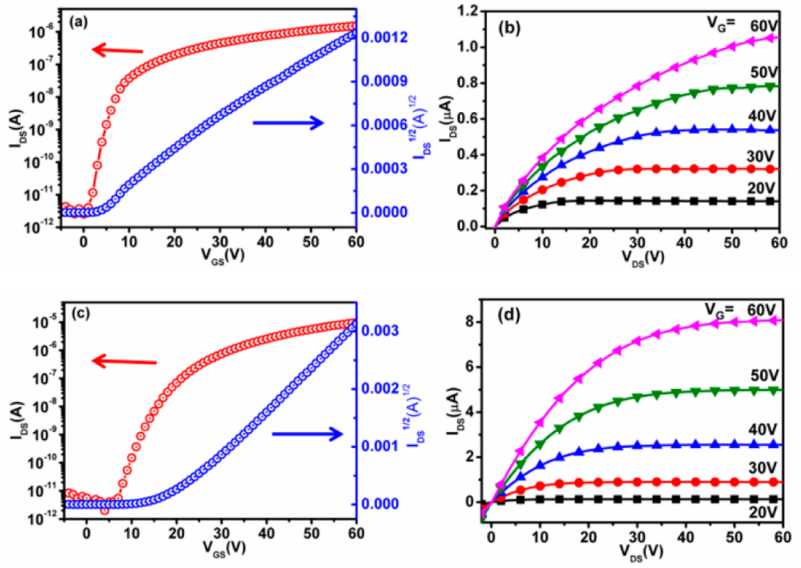

Figure 2. (a) Transfer and (b) output characteristics of $PC_{61}BAd$ OFETs without HMDS modification layer; (c) transfer and (d) output characteristics of $PC_{61}BAd$ OFETs with HMDS modification layer.

Table 1. Parameters of the OFETs Based on $PC_{61}BAd$

SiO_2 layer	μ_e (cm^2/V·s)	I_{on}/I_{off}	V_T (V)
Bare	8.85×10^{-4}	6.0×10^5	3.6
HMDS	0.01	4.9×10^6	18.7

Figure 3 shows the AFM images of the $PC_{61}BAd$ film on the bare Si/SiO_2 layer and the HMDS treated Si/SiO_2 layer. The

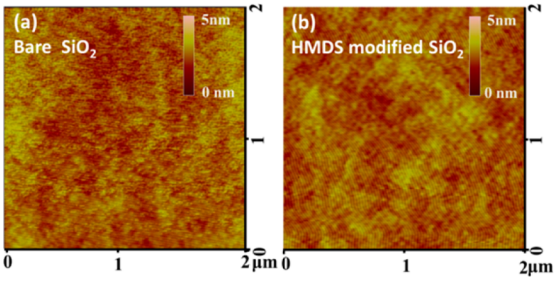

Figure 3. AFM images of the $PC_{61}BAd$ films on (a) bare Si/SiO_2 and (b) HMDS treated Si/SiO_2.

crystallinity and morphology of the two films are quite different. The root-mean-square (RMS) roughness of $PC_{61}BAd$ film on the bare Si/SiO_2 layer is 0.484 nm and small crystals are distributed on the surface. For the HMDS-treated Si/SiO_2 device, the $PC_{61}BAd$ film is even smoother with a RMS of 0.345 nm. Furthermore, much large crystals are found to be distributed on the film. The smooth surface and large crystals in the film can well account for the much enhanced performance of the device with HMDS in comparison to that of the device without HMDS.

For comparison, the OFET devices of $PC_{61}BM$ were also fabricated with HMDS as the modification layer. The optimized device of $PC_{61}BM$ gave an electron saturation mobility of 0.068 cm^2/V·s (see Figure S4 in Supporting Information), which is higher than that of $PC_{61}BAd$. According to the previous report,[9] the electron mobility of the fullerene derivatives is susceptible to small structural alterations and the functional pattern of the addends. Therefore, the lower electron mobility of $PC_{61}BAd$ may be caused by the adamantane group with insulated cage structure that decreases the charge transport in the OFET film. On the other hand, it should be noted that OFET devices of $PC_{61}BAd$ showed higher I_{on}/I_{off} ratio of 4.9×10^6 than that of $PC_{61}BM$ (1.9×10^5). The higher I_{on}/I_{off} ratio would give rise to a better contrast in the $PC_{61}BAd$-based OFET devices and these characteristics are important in logic devices and active matrix display applications.

Photovoltaic Properties. Considering the effect of donor:acceptor ratio on the performance of OSCs being significant,[24−26] the use of optimal donor and acceptor can avoid the charge accumulation and recombination in the bulk heterojunction solar cells so as to balance the electron and hole transport.[27−29] Devices with different donor:acceptor blend ratios (1:1, 1:0.8, 1:0.6, 1:0.4; 15 mg/mL P3HT in DCB) are fabricated. Their $J-V$ characteristics and external quantum efficiencies (EQE) are given in Figure 4a and 4b, respectively. The obtained parameters of the devices are summarized in Table 2. The optimal blend ratio has been demonstrated to be 1:0.6 (P3HT:$PC_{61}BAd$) and the optimal annealing condition involves heating at 110 °C for 10 min in N_2. The PCE of the optimized device reaches 3.31 %, accompanied by a V_{oc} of 0.68 V, a J_{sc} of 7.31 mA/cm^2, and a fill factor (FF) of 66.6 %.

In addition, the J_{sc} values of the P3HT:$PC_{61}BAd$ solar cells are lower than those of the $PC_{61}BM$-based devices (usually ~9 mA/cm^2). This can be rationalized by the corresponding lower electron mobility of $PC_{61}BAd$ as discussed in the OFET studies. However, the P3HT:$PC_{61}BAd$ solar cells showed increased V_{oc}, such as 0.68 V at a ratio of 1:0.6 and 0.71 V at a ratio of 1:0.4, which are higher than those found in the P3HT:$PC_{61}BM$ devices (usually ~0.6 V).[10,11] These, together with the CV data, indicated that $PC_{61}BAd$ has a similar LUMO level as that of $PC_{61}BM$. On the other hand, these results suggest that the V_{oc} in bulk heterojunction solar cells is not only determined by the difference between the highest occupied molecular orbital (HOMO) of the donor and the LUMO of the acceptor, but also depends on other factors.[30] In general, the V_{oc} of organic solar cells can be expressed by the following equation[30]

dx.doi.org/10.1021/am402523n | ACS Appl. Mater. Interfaces 2013, 5, 9579−9584

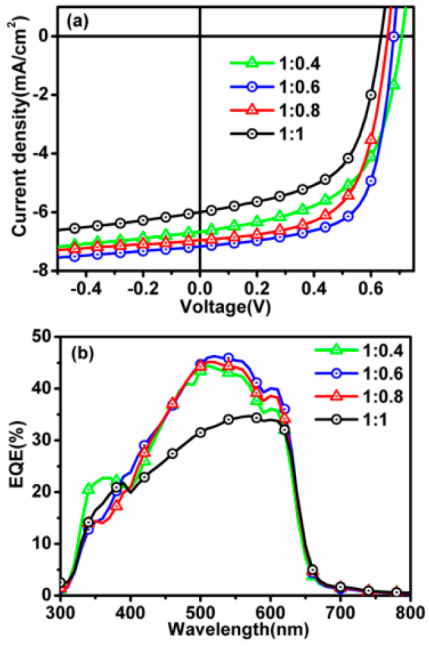

Figure 4. (a) $J-V$ characteristics of P3HT:PC_{61}BAd OSCs and (b) EQE spectra of P3HT:PC_{61}BAd OSCs with different donor: acceptor ratios.

Table 2. Photovoltaic Performance of the P3HT:PC_{61}BAd Devices with Different Ratios

ratio	V_{oc} (V)	J_{sc} (mA/cm^2)	FF (%)	PCE (%)
1:0.4	0.71	6.81	56.4	2.73
1:0.6	0.68	7.31	66.6	3.31
1:0.8	0.66	7.09	62.9	2.94
1:1	0.63	6.11	58.3	2.24

$$V_{oc} = \frac{nkT}{q}\ln\left(\frac{J_{sc}}{J_{so}}\right) + \frac{\Delta E_{DA}}{2q}$$

where k is the Boltzmann's constant, n is the ideality factor, T is the temperature, q is elementary charge, ΔE_{DA} is the donor/acceptor interface energy gap defined by the difference between the HOMO energy of the donor and the LUMO energy of the acceptor, and the value of J_{so} is the current resulting from carriers generated thermally at the D/A interface. The value of J_{so} is quite sensitive to the material properties which determine the thermally generated carriers. For the P3HT:PC_{61}BM and P3HT:PC_{61}BAd systems, though they have the similar ΔE_{DA}, their values of J_{sc}/J_{so} are quite different. Material properties, such as the inter-molecular orbital overlap at the donor/acceptor interface, are one of the main factors influencing the magnitude of J_{sc}/J_{so}. Thus, the enhanced V_{oc} of the P3HT:PC_{61}BAd solar cells would account for the higher values of J_{sc}/J_{so} in their devices.

Thermal Stability. Thermal stability is a critical issue in organic photovoltaic devices. For example, it has been reported that the performance of PC_{61}BM-based OSCs degrades rapidly upon heating.[31−33] The reduced performance is mainly attributed to the fast migration of PC_{61}BM molecules and the resulted PC_{61}BM aggregates.[34−38] In this work, the thermal stability of OSCs constructed by P3HT:PC_{61}BAd is systematically investigated. The optimal P3HT:PC_{61}BAd blend ratio of 1:0.6 was used to fabricate the OPV devices. In addition, the P3HT:PC_{61}BM devices have also been fabricated as reference. The ITO/PEDOT:PSS/blend films are isothermally heated at 150 °C for 0, 5, 10, and 20 h before cathode deposition. The $J-V$ curves of the devices are shown in Figure 5 and the device parameters are listed in Table 3.

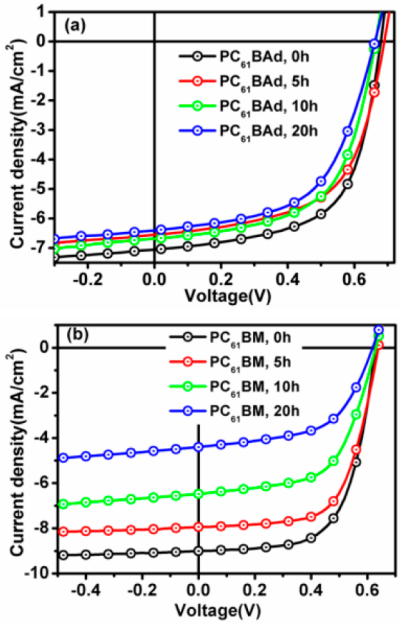

Figure 5. $J-V$ characteristics of (a) P3HT:PC_{61}BAd and (b) P3HT:PC_{61}BM OSCs before and after annealing at 150 °C.

In Figure 5a, it can be clearly seen that the performance of the P3HT:PC_{61}BAd device would degrade as the heating time is increased. The PCE drops from 3.04 % for the unheated sample to 2.44 % for the 20 h-heated sample along with the various V_{oc}, J_{sc} and FF. In comparison, it can be seen from Figure 5b that the PCE of the reference P3HT:PC_{61}BM device deteriorates dramatically with prolongation of heating time, with the PCE reduced from 3.73 % for the un-heated sample to only 1.57 % for the 20 h-heated sample. To clearly compare the deterioration rates of the devices, the PCE of each device with different heating time has been normalized, as shown in Figure S5. It can be clearly seen that as the heating time was extended to 20 h, the P3HT:PC_{61}BM device would display only 42 % of the initial performance, whereas the P3HT:PC_{61}BAd device would still retain 80 % of its initial performance. These results revealed that the addition of the adamantane group in PC_{61}BAd could enhance the thermal stability of the OPV devices, paving the way for the preparation of thermally stable organic solar cells.

From these results, it is apparent that the degradation of these OPV devices is dominated by the reduced J_{sc}. To elucidate the origin for the changes in J_{sc}, optical microscopy (OM) measurements were performed to obtain data on the film morphology. For the OM images (Figure 6), there is no obvious change in the P3HT:PC_{61}BAd films with or without thermal treatment. However, large butterfly-shaped knots (PC_{61}BM crystals) appear in the films, and with longer heating time, more of such knots would be observed.[11,39] In high magnification images (Figure S6), clear PC_{61}BM clusters are observed. This would be attributed to the fact that PC_{61}BM could be driven to undergo fast aggregation during the thermal

Table 3. Photovoltaic Properties of the P3HT:PC_{61}BAd (1:0.6) and P3HT:PC_{61}BM OSCs as a Function of the Annealing Time

acceptor	annealing time (h)	V_{oc} (V)	J_{sc} (mA/cm^2)	FF (%)	PCE (%)	PCE (ave.)[a] (%)
PC_{61}BAd	0	0.68	7.19	62.1	3.04	2.93
	5	0.69	6.67	59.2	2.72	2.67
	10	0.66	6.83	59.3	2.67	2.45
	20	0.66	6.54	56.5	2.44	2.24
PC_{61}BM	0	0.63	9.19	64.4	3.73	3.61
	5	0.64	8.11	64.6	3.35	3.27
	10	0.63	6.59	59.9	2.49	2.32
	20	0.62	4.48	56.6	1.57	1.47

[a]The average values were calculated based on six repeated experiments.

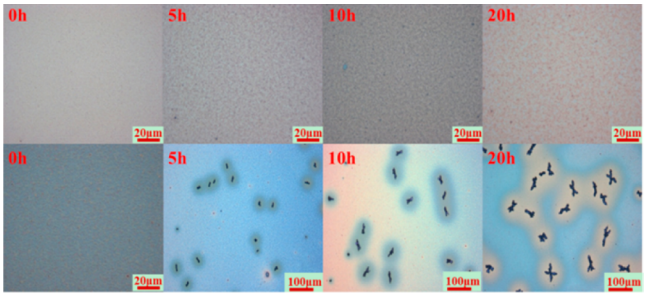

Figure 6. Optical microscope images of P3HT:PC_{61}BAd (top panel) and P3HT:PC_{61}BM (bottom panel) films after thermal annealing at 150 °C with various durations.

treatment. As a result, the initially good donor:acceptor phase separation is considerably destroyed, which leads to a reduced J_{sc} and PCE. Nevertheless, the introduction of adamantane can significantly suppress aggregation, and consequently maintain acceptable OPV performance.

XRD and AFM characterizations were also employed to understand these results (Figure 7). For the unheated

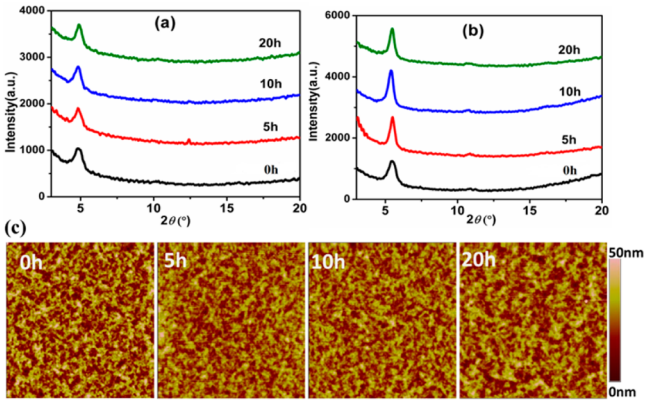

Figure 7. XRD patterns of (a) P3HT:PC_{61}BAd and (b) P3HT:PC_{61}BM blends with different annealing time and (c) AFM images of the P3HT:PC_{61}BAd films with different annealing time (10 μm × 10 μm).

P3HT:PC_{61}BAd film, the XRD pattern displays a diffraction peak at 2θ = 4.89°, while a peak was found at 5.47° for the unheated P3HT:PC_{61}BM film. According to the Bragg's law, the *d*-spacing of P3HT crystallites in the P3HT:PC_{61}BAd film is slightly larger than that in the P3HT:PC_{61}BM film, and this may account for the lower J_{sc} in the unheated P3HT:PC_{61}BAd devices due to the poor intermolecular overlap. During the subsequent heating processes, the XRD pattern of the P3HT:PC_{61}BAd film showed similar peaks, revealing the high thermal stability of this film, which is consistent with the OPV and optical microscopy results. However, for the P3HT:PC_{61}BM film, the XRD patterns displayed an increase in the intensity of the peaks along with the heating time up to 20 h. This showed an increase in the crystallinity of P3HT, which led to the sharply reduced J_{sc} as illustrated in Table 3.

AFM images can further demonstrate the thermal stability of the P3HT:PC_{61}BAd film. As shown in Figure 7c, uniform P3HT:PC_{61}BAd films remained nearly unchanged with increasing time of heating. The morphology of the four films displays similar RMS (6.5, 5.4, 5.4, and 6.1 nm for 0, 5, 10, and 20 h, respectively). However, for P3HT:PC_{61}BM films, large PC_{61}BM crystals appeared after heat treatment as shown by optical microscopy in Figure 6, and the formation of these aggregates even prevented AFM detection. Moreover, the aggregation of PC_{61}BM would lead to fast crystallization of P3HT, finally destroying the P3HT/PC_{61}BM interfaces as well as the pathway for carrier transport. Thus, in comparison to the P3HT:PC_{61}BM device, the P3HT:PC_{61}BAd devices possess good thermal stability even after a long-term heat treatment.

CONCLUSIONS

In summary, an adamantane-containing fullerene derivative, PC_{61}BAd, has been designed and synthesized. The PC_{61}BAd-based OFETs exhibit an electron mobility of 0.01 cm^2/V·s and a high I_{on}/I_{off} ratio of 4.9 × 10^6. The P3HT:PC_{61}BAd OSCs achieve a PCE of 3.31 %, with V_{oc} of 0.68 V and FF of 66.6 %. Moreover, PC_{61}BAd-based OPV devices display superior thermal stability over that of the PC_{61}BM devices. After heating at 150 °C for 20 h, the P3HT:PC_{61}BM device showed only 42 % of the initial performance, whereas the P3HT:PC_{61}BAd device still retained 80 % of its initial performance. The present work has provided a promising fullerene material for applications in electronic devices and solar cells.

ASSOCIATED CONTENT

Supporting Information

Description of the synthesis, NMR, CV, UV−vis absorption spectra, and the OM pictures. This material is available free of charge via the Internet at http://pubs.acs.org.

AUTHOR INFORMATION

Corresponding Authors

*E-mail: wangtais@iccas.ac.cn.
*E-mail: jczheng@xmu.edu.cn.
*E-mail: wwyam@hku.hk.

Notes

The authors declare no competing financial interest.

■ ACKNOWLEDGMENTS

V.W.-W.Y. acknowledges support from The University of Hong Kong under URC Strategic Research Theme on New Materials. This work has been supported by the Theme-Based Research Scheme of the Research Grants Council of Hong Kong (Project no. T23-713/11). T.W. acknowledges support from the China Postdoctoral Science Foundation (201104153) and Hong Kong Scholars Program. J.-C.Z. acknowledges support from the Minjiang Scholar Distinguished Professorship Program through Xiamen University of China and Specialized Research Fund for the Doctoral Program of Higher Education (20090121120002 and 20100121120026).

■ REFERENCES

(1) Günes, S.; Neugebauer, H.; Sariciftci, N. S. *Chem. Rev.* **2007**, *107*, 1324−1338.
(2) Arias, A. C.; MacKenzie, J. D.; McCulloch, L.; Rivnay, J.; Salleo, A. *Chem. Rev.* **2010**, *110*, 3−24.
(3) Cheng, Y. J.; Yang, S. H.; Hsu, C. S. *Chem. Rev.* **2009**, *109*, 5868−5923.
(4) Chen, L. M.; Hong, Z.; Li, G.; Yang, Y. *Adv. Mater.* **2009**, *21*, 1434−1449.
(5) Dennler, G.; Scharber, M. C.; Brabec, C. J. *Adv. Mater.* **2009**, *21*, 1323−1338.
(6) Jorgensen, M.; Norrman, K.; Gevorgyan, S. A.; Tromholt, T.; Andreasen, B.; Krebs, F. C. *Adv. Mater.* **2012**, *24*, 580−612.
(7) Thompson, B. C.; Frechet, J. M. *Angew. Chem., Int. Ed.* **2008**, *47*, 58−77.
(8) Chen, J.; Cao, Y. *Acc. Chem. Res.* **2009**, *42*, 1709−1718.
(9) Li, C. Z.; Chueh, C. C.; Yip, H. L.; Zou, J.; Chen, W. C.; Jen, A. K. Y. *J. Mater. Chem.* **2012**, *22*, 14976−14981.
(10) He, Y. J.; Chen, H. Y.; Hou, J. H.; Li, Y. F. *J. Am. Chem. Soc.* **2010**, *132*, 1377−1382.
(11) Meng, X. Y.; Zhang, W. Q.; Tan, Z. A.; Li, Y. F.; Ma, Y. H.; Wang, T. S.; Jiang, L.; Shu, C. Y.; Wang, C. R. *Adv. Funct. Mater.* **2012**, *22*, 2187−2193.
(12) Cheng, Y. J.; Liao, M. H.; Chang, C. Y.; Kao, W. S.; Wu, C. E.; Hsu, C. S. *Chem. Mater.* **2011**, *23*, 4056−4062.
(13) Anthopoulos, T. D.; Tanase, C.; Setayesh, S.; Meijer, E. J.; Hummelen, J. C.; Blom, P. W. M.; Leeuw, D. M. *Adv. Mater.* **2004**, *16*, 2174−2179.
(14) Singh, T. B.; Marjanović, N.; Stadler, P.; Auinger, M.; Matt, G. J.; Günes, S.; Sariciftci, N. S.; Schwödiauer, R.; Bauer, S. *J. Appl. Phys.* **2005**, *97*, 083714−083718.
(15) Reyes-Reyes, M.; Kim, K.; Carroll, D. L. *Appl. Phys. Lett.* **2005**, *87*, 083506−083508.
(16) Ma, W. L.; Yang, C. Y.; Gong, X.; Lee, K.; Heeger, A. J. *Adv. Funct. Mater.* **2012**, *22*, 2187−2193.
(17) Archibald, T. G.; Malik, A. A.; Baum, K.; Unroe, M. R. *Macromolecules* **1991**, *24*, 5261−5265.
(18) Khardin, A. P.; Radchenko, S. S. *Russ. Chem. Rev.* **1982**, *51*, 272−285.
(19) Han, D. W.; Moore, J. A. *Polymer* **2009**, *50*, 2551−2557.
(20) Dimitrakopoulos, C. D.; Malenfant, P. R. L. *Adv. Mater.* **2002**, *14*, 99−117.
(21) Chua, L. L.; Zaumseil, J.; Chang, J. F.; Ou, E. C. W.; Ho, P. K. H.; Sirringhaus, H.; Friend, R. H. *Nature* **2005**, *434*, 194−199.
(22) Chua, L. L.; Ho, P. K. H.; Sirringhaus, H.; Friend, R. H. *Appl. Phys. Lett.* **2004**, *84*, 3400−3402.
(23) Horii, Y.; Ikawa, M.; Chikamatsu, M.; Azumi, R.; Kitagawa, M.; Konishi, H.; Yase, K. *ACS Appl. Mater. Interfaces* **2011**, *3*, 836−841.
(24) Liang, Y.; Xu, Z.; Xia, J.; Tsai, S. T.; Wu, Y.; Li, G.; Ray, C.; Yu, L. *Adv. Mater.* **2010**, *22*, E135−E138.
(25) Saravanan, C.; Liu, C. L.; Chang, Y. M.; Lu, J. D.; Hsieh, Y. J.; Rwei, S. P.; Wang, L. *ACS Appl. Mater. Interfaces* **2012**, *4*, 6133−6141.
(26) Pan, J. Y.; Zuo, L. J.; Hu, X. L.; Fu, W. F.; Chen, M. R.; Fu, L.; Gu, X.; Shi, H. Q.; Shi, M. M.; Li, H. Y.; Chen, H. Z. *ACS Appl. Mater. Interfaces* **2013**, *5*, 972−980.
(27) Koster, L. J. A.; Mihailetchi, V. D.; Blom, P. W. M. *Appl. Phys. Lett.* **2006**, *88*, 052104−052106.
(28) Wagenpfahl, A.; Rauh, D.; Binder, M.; Deibel, C.; Dyakonov, V. *Phys. Rev. B* **2010**, *82*, 115306−115313.
(29) Peumans, P.; Forrest, S. R. *Chem. Phys. Lett.* **2004**, *398*, 27−31.
(30) Perez, M. D.; Borek, C.; Forrest, S. R.; Thompson, M. E. *J. Am. Chem. Soc.* **2009**, *131*, 9281−9286.
(31) Meng, X. Y.; Zhang, W. Q.; Tan, Z. A.; Du, C.; Li, C. H.; Bo, Z. S.; Li, Y. F.; Yang, X. L.; Zhen, M. M.; Jiang, F.; Zheng, J. P.; Wang, T. S.; Jiang, L.; Shu, C. Y.; Wang, C. R. *Chem. Commun.* **2012**, *48*, 425−427.
(32) Cheng, Y. J.; Hsieh, C. H.; Li, P. J.; Hsu, C. S. *Adv. Funct. Mater.* **2011**, *21*, 1723−1732.
(33) Zhang, Y.; Yip, H. L.; Acton, O.; Hau, S. K.; Huang, F.; Jen, A. K. Y. *Chem. Mater.* **2009**, *21*, 2598−2600.
(34) Yang, X. N.; Duren, J. K. J.; Rispens, M. T.; Hummelen, J. C.; Janssen, R. A. J.; Mickels, M. A. J.; Loos, J. *Adv. Mater.* **2004**, *16*, 802−806.
(35) Müller, C.; Ferenczi, T. A. M.; Campoy-Quiles, M.; Frost, J. M.; Bradley, D. D. C.; Smith, P.; Stingelin-Stutzmann, N.; Nelson, J. *Adv. Mater.* **2008**, *20*, 3510−3515.
(36) Yang, X. N.; Duren, J. K. J.; Janssen, R. A. J.; Michels, M. A. J.; Loos, J. *Macromolecules* **2004**, *37*, 2151−2158.
(37) Vandenbergh, J.; Conings, B.; Bertho, S.; Kesters, J.; Spoltore, D.; Esiner, S.; Zhao, J.; Van Assche, G.; Wienk, M. M.; Maes, W.; Lutsen, L.; Van Mele, B.; Janssen, R. A. J.; Manca, J.; Vanderzande, D. J. M. *Macromolecules* **2011**, *44*, 8470−8478.
(38) Swinnen, A.; Haeldermans, I.; Ven vande, M.; D'Haen, J.; Vanhoyland, G.; Aresu, S.; D'Olieslaeger, M.; Manca, J. *Adv. Funct. Mater.* **2006**, *16*, 760−765.
(39) Li, C. Z.; Chien, S. C.; Yip, H. L.; Chueh, C. C.; Chen, F. C.; Matsuo, Y.; Nakamura, E.; Jen, A. K. Y. *Chem. Commun.* **2011**, *47*, 10082−10084.
(40) Ma, W. L.; Yang, C. Y.; Gong, X.; Lee, K. H.; Heeger, A. J. *Adv. Funct. Mater.* **2005**, *15*, 1617−1622.